

Effective Constant of Porous Materials Using Micro-Meso Damage Modeling

Nabi Mehri Khansari^{1}, Seyed Mohammad Navid Ghoreishi², Ayad Al-Rumaithi³*

1 Faculty of mechanical Engineering, Sahand University of Technology, Tabriz, Iran

2 Satellite Research Institute, Iranian Space Research Center, Tehran, Iran

3 Department of Civil Engineering, University of Baghdad, Iraq

ABSTRACT: Take in to account of metal foams properties like energy absorption; they have several implementations. The complication of foam structures leads difficulties in investigation of elastic and plastic modulus. In the present research, porosity of foam are modeled and analyzed, numerically. In this context, MATLAB and JavaScript have been developed for geometrical modeling of porous materials considering density, radius, and random distribution of porous. Several porous configurations are simulated using periodic boundary conditions on Micro/Meso Scale in order to numerically calculate their elastic mechanical properties like Young's modulus and shear modulus as a function of the porous configuration. The porous are distributed randomly and the effect of configuration parameters (like shape, number, size) are investigated on elastic modulus. In order to simulate more accurately, porous characteristics were investigated using SEM experimental tests. Eventually, the calculated effective constants of porous materials are compared with numerical and experimental literatures. This comparison demonstrates that the proposed method can accurately model high range of porosity (from 5% to 65%) and estimate the effective constant of porous materials in 3 directions including of (E1, E2, E3, G12, G13, G23).

KEYWORDS: *Aluminum foam, porous material, Mechanical properties, Micro-Meso scale, Numerical Analysis*

INTRODUCTION

Foam structures are implemented in several industries due to their significant mechanical features like low-density, high porosity, light weighting and high energy absorption[1, 2]. There are various applications of foam structures like sandwich panel core[3] or special application of

electromagnetic [4], sound[5] and energy[6, 7]. Foams are included some discontinuity called cells or porous and the mechanical behaviors of foams are influenced by the shape and densities of cells [8-11]. However, noteworthy characteristics of [1-3] make them so applicable and totally divided them in to different materials such as non-metal-based (e.g. polyvinyl chloride (PVC) froth) and metal-based (e.g. aluminum) compounds. [8-13]. The Aluminum foam is applied in various industries such as aerospace, civil, and communication technologies. Indeed, both high specific mechanical properties, and electromagnetic [4], sound [5] and energy [6, 7] absorption have been obtained using aluminum foams. Sandwich panel is also another implementation of these foams. In this context, the impact response of aluminum foam has been researched as well as

fracture and damage. Also, fracture of open and close metal foams such as nickel-chromium and 6101 aluminum foams were considered in which failure process were observed. The mechanical behavior of foams is affected by some parameters such as the shape of vacancies and the densities of vacancies or cellular structures. Although foams generally indicate high strength in compression loading, they suffer from low consistency in tensile loading.

Regarding the porosity of foams, mechanical properties of these materials depend on the size, shape, and location of porosities[14, 15]. Cells or pores are randomly distributed in solid foam and can have regular (e.g. spherical and elliptical shape) or irregular (e.g. defect) shape (Figure1). In the present research, it is supposed to introduce a method for simulation of mechanical properties of foam structures, considering random distribution of cells or pores. In this context, some theoretical methods have proposed for modeling of porous media in foams. For instance, the differential effective medium approach (DEMA) is one of the helpful methods.

* Corresponding author's email: n.mehri@sut.ac.ir
Tel.: +989129214770

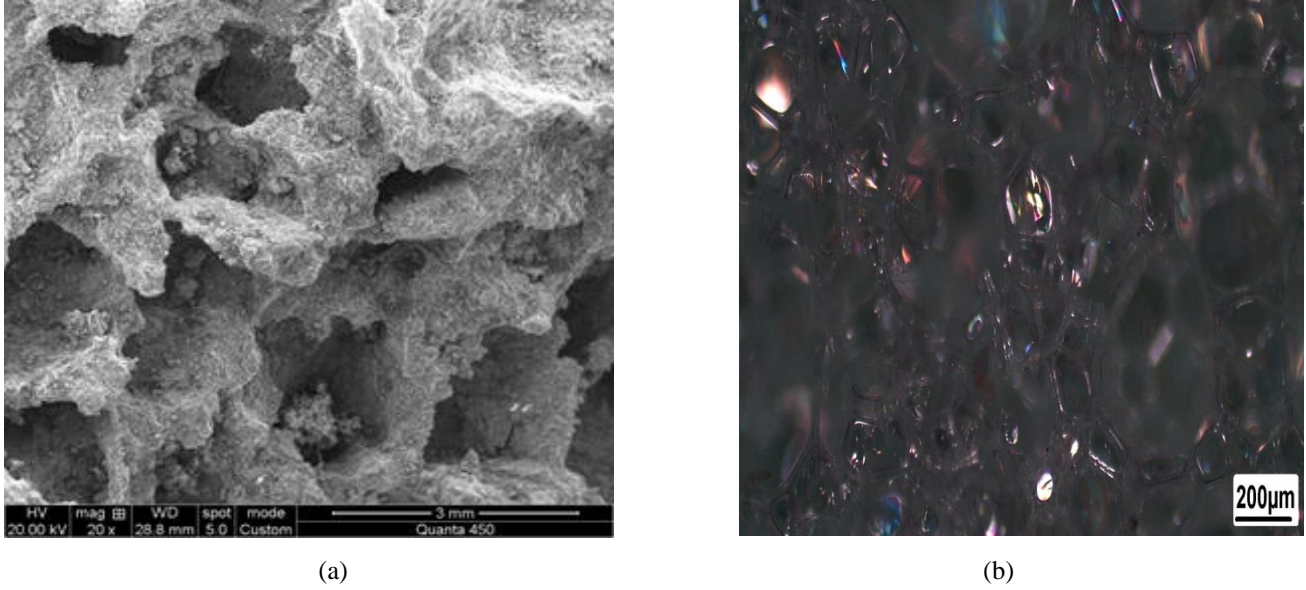


Fig. 1. Irregular and random shape of porous (cell) in the aluminum (a) and PVC foam, SEM investigation in the present study

The DEMA was first proposed by Bruggeman [16] based on elastic modulus and shear modulus. Since, the Bruggeman theory is not convenience to use for finite concentration of pores, incredibly porous interaction, Boccaccini [17] proposed an empirical-based method for spherical pores. Rajinder Pal [18] also introduced a developed method based on the Bruggeman theory. Mooney [19] proposed an incremental-based method for investigation of porous solids. Similar research was done by Krieger and Dougherty [20] where the volume fraction of the porous could grow similar to the Mooney method. Both spherical [21] as well as elliptical [22-27] cells and irregular shapes of cells such as micro-defects [28-30] can play a significant role in the overall mechanical behavior of isotropic foam. It can also be simulated based on porosity type and its interaction.

On the other hand, in the context of interacting, the effective properties could be evaluated by performing self-consistent method (SCM) [28], Mori-Tanaka method [31], differential method [32], generalized self-consistent method (GSCM) [33, 34] and X.Q. Feng [35]. The effective elastic and shear moduli were also classified in the basis of cracked composite's structures [36]. In this context, an approach was established to present the material properties considering damage zone (at crack tip vicinity) [37-40].

In the Table 1, some recent methods of obtaining the Effective modulus of porous materials are mentioned based on micromechanics and DEMA concepts. These methods are usually based on the porosity density of cubic formation of cells as $\varepsilon = na^3$ [40, 41].

Table 1. Effective modulus of porous materials based on micromechanics and DEMA concepts

| Authors | Concepts | $\left(\frac{\bar{G}}{G}\right)$ | $\left(\frac{\bar{E}}{E}\right)$ |
|----------------------------|------------------------------|---|---|
| Bruggeman [16] | DEMA | $exp\left(-\frac{5}{3}\varepsilon\right)$ | $exp\left(-\frac{23}{12}\varepsilon\right)$ |
| Boccaccini [17] | DEMA | $(1 - \varepsilon)^{\frac{5}{3}}$ | $(1 - \varepsilon)^{\frac{23}{12}}$ |
| Mooney [19] | DEMA | $exp\left(\frac{\left(-\frac{5}{3}\right)\varepsilon}{1 - \left(\frac{\varepsilon}{\varepsilon_m}\right)}\right)$ | $exp\left(\frac{\left(-\frac{23}{12}\right)\varepsilon}{1 - \left(\frac{\varepsilon}{\varepsilon_m}\right)}\right)$ |
| Krieger and Dougherty [20] | DEMA | $\left(1 - \left(\frac{\varepsilon}{\varepsilon_m}\right)\right)^{\left(\frac{5}{3}\right)\varepsilon_m}$ | $\left(1 - \left(\frac{\varepsilon}{\varepsilon_m}\right)\right)^{\left(\frac{23}{12}\right)\varepsilon_m}$ |
| Budiansky et al. [42] | Self-consistent method (SCM) | $1 - \frac{32(1 - \bar{\nu})(5 - \bar{\nu})}{45(2 - \bar{\nu})}\varepsilon$ | $1 - \frac{16(1 - \bar{\nu}^2)(10 - 3\bar{\nu})}{45(2 - \bar{\nu})}\varepsilon$ |

| | | | |
|----------------------|---|---|--|
| Hashin et al. [43] | Differential scheme method (DSM) | $\frac{\bar{E}}{E} \left(\frac{1+v}{1+\bar{v}} \right)$ | $\left(\frac{\bar{v}}{v} \right)^{\frac{10}{9}} \left(\frac{3-v}{2-\bar{v}} \right)^{\frac{1}{9}}$ |
| Huang et al, [44] | Generalized self-consistent method (GSCM) | $\left[1 - \frac{32(1-v)(5-v)\varepsilon}{45(2-v)} + D_G(v)\varepsilon^{-\frac{5}{2}} \right]^{-1}$ | $\left[1 + \frac{16(1-v^2)(10-3v)\varepsilon}{45(2-v)} + D_E(v)\varepsilon^{-\frac{5}{2}} \right]^{-1}$ |
| Krajcinovic, [45] | Dilute concentration method (DCM) | $\left[1 + \frac{32(1-v)(5-v)\varepsilon}{45(2-v)} \right]^{-1}$ | $\left[1 + \frac{16(1-(v^2))(10-3v)\varepsilon}{45(2-v)} \right]^{-1}$ |
| Feng et al, [46] | Effective self-consistent method (FENG) | $\left[1 + \frac{32(1-v)(5-v)\varepsilon}{45(2-v)(1-\xi\varepsilon^\eta)} \right]^{-1}$ | $\left[1 + \frac{16(1-(v^2))(10-3v)\varepsilon}{45(2-v)(1-\xi\varepsilon^\eta)} \right]^{-1}$ |
| Fakoor and Mehri[47] | Representative Circular Elements (RCE) | $\left[1 + \frac{32(1-\bar{v})(5-\bar{v})\varepsilon}{45(2-\bar{v})(1-\gamma\varepsilon)} \right]^{-1}$ | $\left[1 + \frac{16(1-\bar{v}^2)(10-3\bar{v})\varepsilon}{45(2-\bar{v})(1-\gamma\varepsilon)} \right]^{-1}$ |
| Mehri et al,[14] | damage zone micro-mechanical criterion (DZMC) | $\frac{-1}{\left[(\bar{S}_{16} + \bar{S}_{26}) \left(\tan \varphi + \frac{2q}{(q^* - q) \sin 2\varphi} \right) + \bar{S}_{66} \right]}$ | $(1 - \varepsilon \bar{S}_{11})$ |

Where, $\frac{\bar{E}}{E}$, $\frac{\bar{G}}{G}$, and ε denote the effective elastic, shear moduli of the pore-solid, and the porous density, respectively. Also, the ε_m , v and \bar{v} denote as the maximum packing volume fraction of spherical pores [19], Poisson's Ratio and damaged Poisson's Ratio, respectively. The Poisson's ratio of porous section of materials has been mentioned in Ref. [47]. Based on the table, shear and elastic moduli of porous materials have been evaluated based on pore density (ε). S_{ij} ($i,j=1,2,3,4,5,6$), q and φ are compliance matrix and random porous configuration, respectively [14]. As it was mentioned, most of the researches present analytical approach in which the pores are modeled by analytical methods, while, the methods should be verified by the experimental and numerical methods. In addition, the presented analytical methods mainly do not have the ability to distribute pores with arbitrary and random shapes, and only circular and elliptical distributions have been investigated. While in reality, the shape, size and position of the pores have a completely random distribution. Therefore, in the present research, a numerical method based on the random distribution of pores has been considered, which can express the random distribution of pores in foams and can be compared and verified with analytical and experimental methods. In other words, the porous are distributed randomly and the effect of configuration parameters (like shape, number, size) are investigated on elastic modulus.

Numerical Modeling of Porous

In the present research, porous is modeled by two method of aggregation and FEA model. In the aggregation method, random shape of porous are simulated using generation, and placement coding in MATLAB software. On the other hand, JavaScript in ANSYS is considered to randomly distribute porous region.

Modeling of Porous: Aggregation Method

The pores in closed cell metal foam can be geometrically simulated as randomly oriented ellipsoids. These ellipsoids

are not intersected with each other, and the their spatial distribution and volumetric proportions should represent realistic material properties[48]. In this paper, the procedure used for modeling aggregate in concrete was modified to generate the pores in the metal foam specimens. The algorithm that was excuted in MATLAB and is divided into two parts: Generation, and Placement. In Generation, the size and the number of ellipoids were calculated according to predefined volumetric distribution for each diameter. Then later in Placement, the position and orientation of each individual ellipsoid were selected after checking that they lie in the specimen boundaries and not intersecting with other ellipoids. These two processes are explained in the following subsections.

Generation and Placement

In order to get realistic representation of the structure of metal foam, the size distribution of pores was taken into account by dividing the ellipsoids into classes according to their diameters. The total volume of ellipsoids for each class should be chosen to represent real specimen. The principal radii of each ellipoids within each class are determined from the following random variable equations [49-52]:

$$d_{eqv} = 2 * r_2 = \frac{d_i d_{i+1}}{\sqrt{u_2 d_i^3 + (1 - u_2) d_{i+1}^3}} \quad (5)$$

$$r_1 = \left(1 + u_1 * \frac{m-1}{m+1} \right) * r_2 \quad (6)$$

$$r_3 = \left(1 - u_3 * \frac{m-1}{m+1} \right) * r_2 \quad (7)$$

where d_{eqv} is the medium diameter, and the prinical radii are r_1 , r_2 , and r_3 with $r_1 \geq r_2 \geq r_3$. d_i and d_{i+1} are the diameter range for the i th diameter class. u_1 , u_2 , and u_3 are the realizations of uniform random variables ranging from 0 to 1. m is a flatness parameter. If its value is 1 the pores are sphere, and if its value is higher than 1 the flatness increases.

This process is summarized as: the volume for largest diameter class is selected. Then individual ellipsoids are generated within that class using equations 1 to 3. This step is repeated until the cumulative volume of ellipsoids exceed the assigned volume for the class. The difference between the assigned and simulated volume is subtracted from the next class. The process is repeated for the smaller classes, descendingly. Similarly to Generation, in Placement the aggregates are placed from the largest to smallest diameter classes. The position and orientation for each individual ellipsoid are randomly chosen within the required domain and checked for the following overlaps[49]: The ellipsoid is checked that it lies within the required specimen geometry.

Then, the overlap between that ellipsoid and nearby ellipsoids are investigated. If there is intersection with geometry boundaries or other ellipsoids, the position and orientation are chosen again. The process is repeated for the other ellipsoids within this diameter class and then for smaller classes.

Different porous dispersions are assumed as particle distribution. In this context, congruential random number generator (multiplicative) [50] and fuller function [51, 52] are the most general theories for random distribution. Random circular and elliptical pore are simulated as vacant modulus particles (blue part) based on pore to intact ratio (porous ratio).

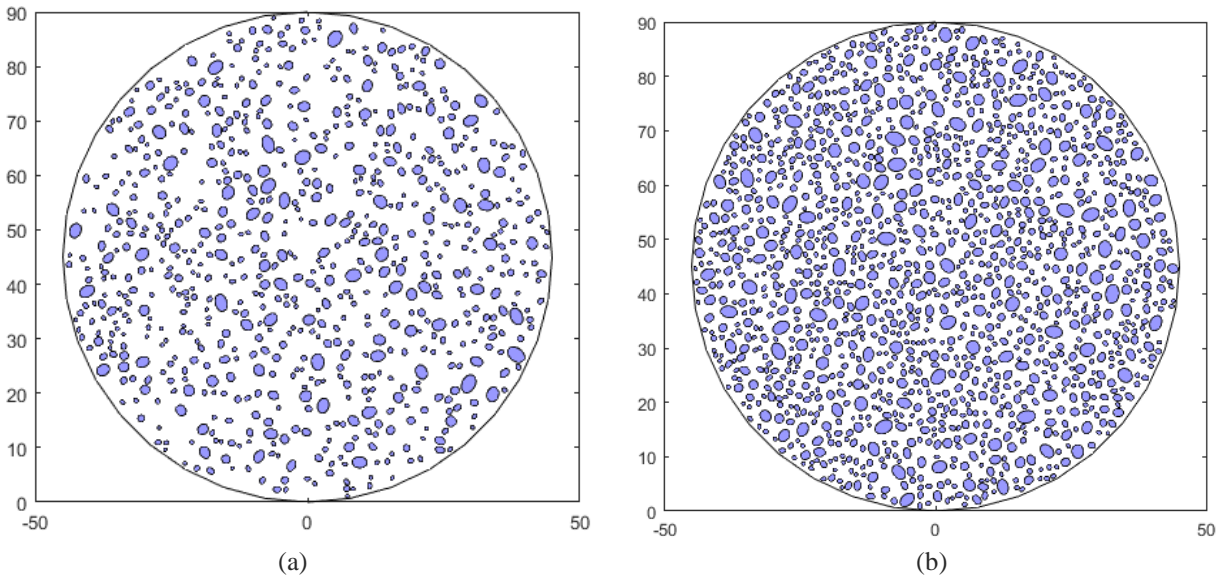


Fig. 2. (a) and (b) illustrating the porous distribution for porous ratio of (0.32) and (0.62), respectively

Also, three dimensional analyses were made based on spherical and ellipsoidal shape of porous.

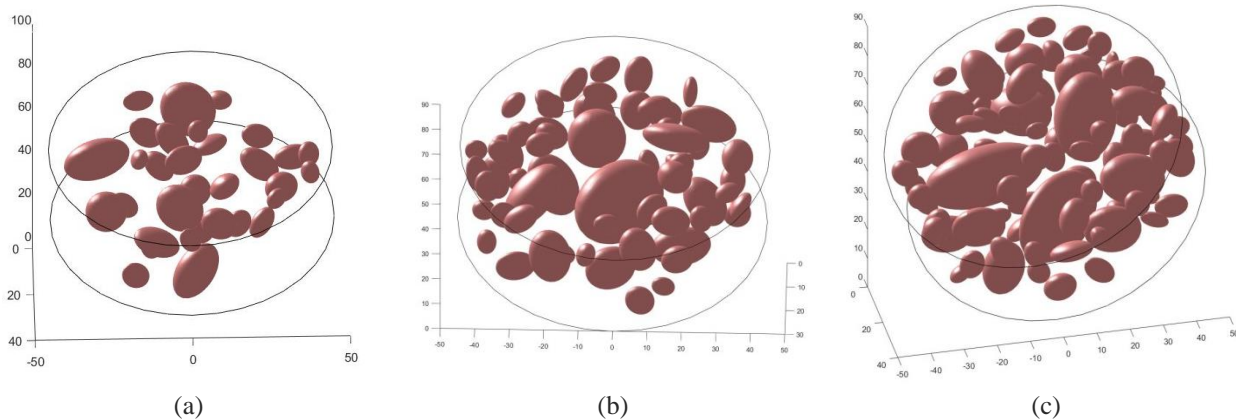


Fig. 3. (a), (b) and (c) represent as 0.2, 0.4 and 0.6 porous ratio distribution

Therefore, the probability function can be obtained based on porous distribution.

Modeling of Porous: FEA Method

One of the most challenging parts of analyzing porous materials is creating an accurate geometric model of the

material. Geometric modeling of porous materials is difficult for several reasons, including the pores' high density, varying radius, and seemingly random distribution. This article presents a method for the geometric modeling of porous materials using MATLAB and JavaScript in tandem with ANSYS. To this end, a MATLAB script was written to generate the porous centers in a cubic geometry. Each pore's position and simulated radius are chosen randomly within a predetermined tolerance range. This script ensures that porous never overlap by setting the minimum distance

criterion to twice the radius. This script also allows the user to adjust the size of the boundary cube, the sphere's radius, and the total number of spheres used in porous material simulations. As a final step, the MATLAB script exports its generated points to a text file that the ANSYS program can read. This allows geometric modeling to be performed in ANSYS based on the locations of the points. The following diagram depicts the logic used by the MATLAB script to determine the porous centers.

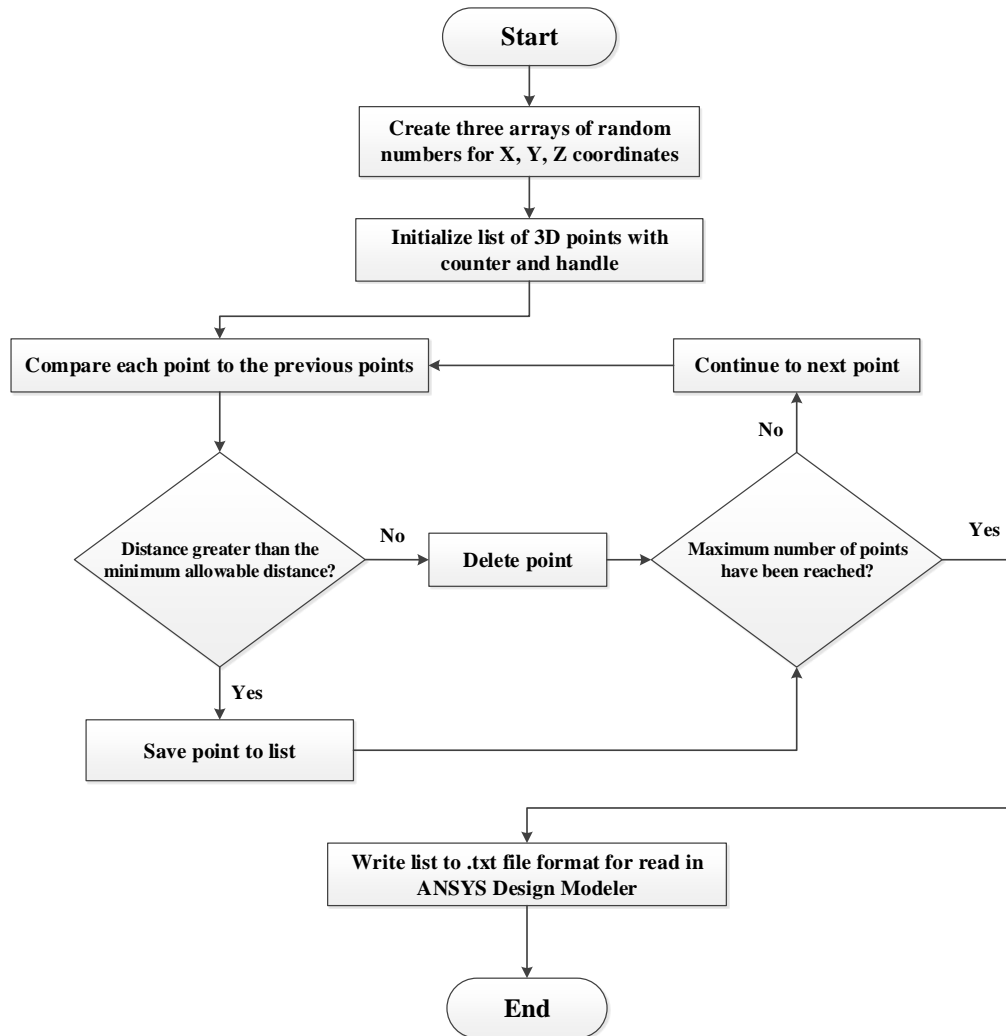


Fig. 4. MATLAB script flowchart for pore center points

In the figure below, a view of the randomly generated points representing the three-dimensional coordinates of the

porous centers by the MATLAB script is shown for the porosity percentage of 20 and 40%.

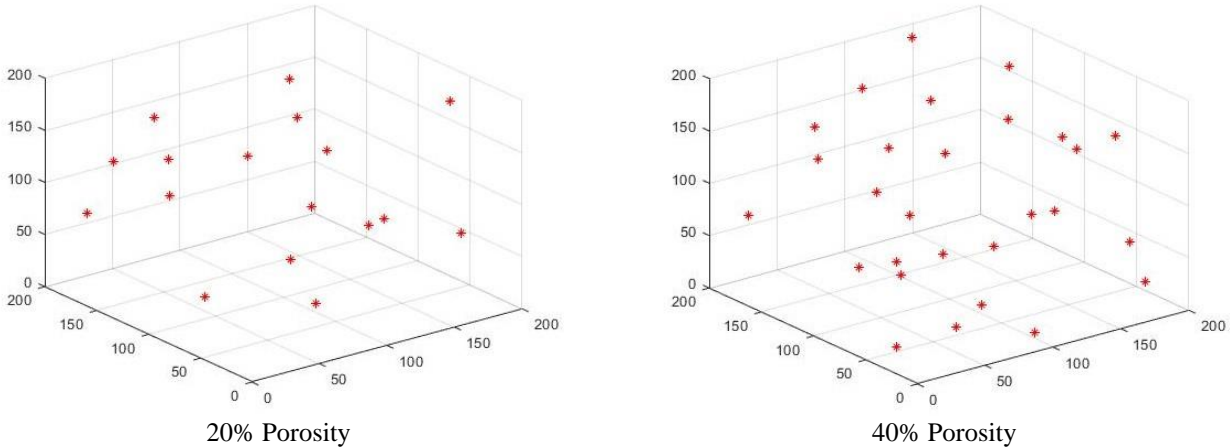


Fig. 5. A view of the randomly generated points representing the three-dimensional coordinates of the porous centers by the MATLAB script for the porosity percentage of 20 and 40%

The geometric drawing of porous materials in ANSYS software can be automated with the help of Java script. To model porous materials in ANSYS, this script reads in the MATLAB script's text file containing the porous centers' three-dimensional coordinates. It produces the three-dimensional geometry of the representative volume element (RVE). The representative volume element (RVE) used to model porous materials is designed to have as small of

dimensions as possible in order to reduce the number of calculations required. The SEM images in reference [48, 53] suggest that a cubic volume element with porous on all sides should have dimensions of $200\ \mu\text{m} \times 200\ \mu\text{m} \times 200\ \mu\text{m}$. The porous radii are also assumed to be chosen at random between $5.0\ \mu\text{m}$ and $3\ \mu\text{m}$. See how ANSYS software handles geometric modeling of porous materials with 20, 30, and 40% porosity in the figure below.

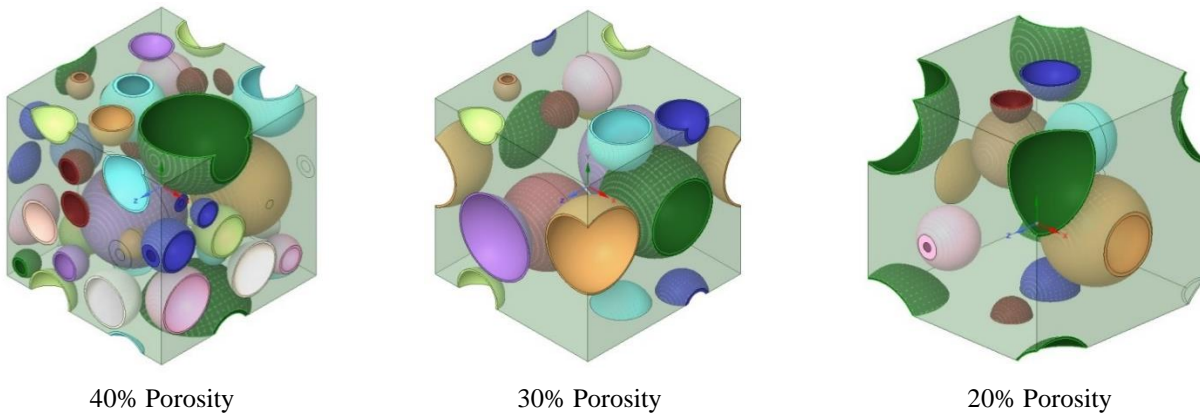


Fig. 6. ANSYS geometry modeling of porous materials with 20, 30, and 40% porosity

Porous Material Finite Element Analysis and Mechanical Property Calculation

To determine the mechanical properties of porous materials, first constructing a geometric model and then developing a finite element model of the desired representative volume element (RVE) is necessary. A finite element model and numerical solutions were developed in ANSYS and used to determine mechanical properties. Idealized calculations are used to determine the mechanical properties of porous materials. This means that local buckling and residual stress in porous materials [54] are not considered when calculating mechanical properties or manufacturing defects. The

quadratic interpolation element with tetrahedral elements has been used to create the finite element model of the required representative volume element (RVE) because of its good performance and appropriate accuracy for complex geometries. Mesh sensitivity analysis is used to determine the optimal element count. The number of constituents needed is proportional to the porosity percentage. RVE finite element modeling with 20% porosity has used 123,000 elements. The figure below depicts the finite element model of porous materials in ANSYS software with 20%, 30%, and 40% porosity percentages.

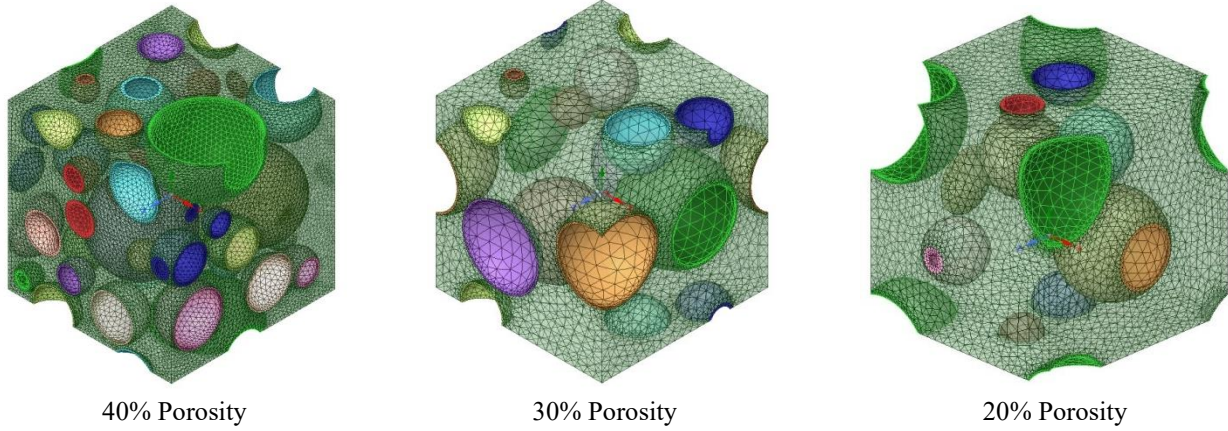


Fig. 7. ANSYS finite element model of porous materials with 20, 30, and 40% porosity

The homogenization method was used for the mechanical property calculations. Here, the Hooke-Lamé law and the stress $(\sigma = (\sigma_{xx}\sigma_{yy}\sigma_{zz}\tau_{yz}\tau_{zx}\tau_{xy})^T)$ and strain $(\varepsilon = (\varepsilon_{xx}\varepsilon_{yy}\varepsilon_{zz}\gamma_{yz}\gamma_{zx}\gamma_{xy})^T)$ values are utilized to derive the stiffness matrix:

$$\sigma = C\varepsilon \quad (8)$$

Combining the three axial strains and three shear strains shown in Figure with periodic boundary conditions allows for calculating the homogeneous response. The corresponding column of i is calculated from the stiffness matrix of C for each unit strain field applied to RVE. In fact, the equilibrium stress vector σ_i for a given strain field ε_i is represented in each column of the stiffness matrix.

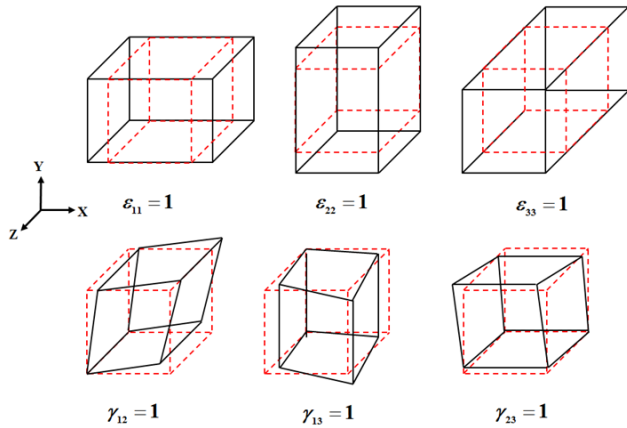


Fig. 8. Schematic design of six-unit strain fields (three pure axial strains and three pure shear strains) to calculate homogeneous stiffness matrix

The analyzed volume must meet both of the following [55] for the stiffness matrix to be computed when periodic boundary conditions are applied to an RVE:

1) The stress field must be periodic for static equilibrium of the RVE.

2) The deformation of the RVE's two opposing sides must be constant.

The above requirements can only be satisfied if the numerical model's geometry and mesh are perfectly symmetrical. In this regard, this paper's geometry and finite element model are symmetrical. The original cell's reflection in the XY, XZ, and YZ planes ensures this symmetry.

$$[S] = [C]^{-1} \quad (9)$$

After calculating the stiffness matrix using the method described, the flexibility matrix must be computed as follows:

$$[S] = \begin{bmatrix} \frac{1}{E_1} & -\frac{\nu_{21}}{E_2} & -\frac{\nu_{31}}{E_3} & 0 & 0 & 0 \\ -\frac{\nu_{12}}{E_1} & \frac{1}{E_2} & -\frac{\nu_{32}}{E_3} & 0 & 0 & 0 \\ -\frac{\nu_{13}}{E_1} & -\frac{\nu_{23}}{E_2} & \frac{1}{E_3} & 0 & 0 & 0 \\ 0 & 0 & 0 & \frac{1}{G_{23}} & 0 & 0 \\ 0 & 0 & 0 & 0 & \frac{1}{G_{13}} & 0 \\ 0 & 0 & 0 & 0 & 0 & \frac{1}{G_{12}} \end{bmatrix} \quad (10)$$

Figure 10 summarizes the steps required to calculate the mechanical properties of porous materials using the method presented in this article. To calculate the mechanical properties of porous materials, the following six steps must be taken according to this diagram:

First step: Create a three-reference plane symmetrical finite element model of RVE.

Second step: Add periodic boundary conditions to the model with nodes.

Third step: Applying six independent unit strain fields to the model.

Fourth step: Calculate each stiffness matrix column using node stresses.

Fifth step: Calculating flexibility matrix from the stiffness matrix.

Sixth step: Mechanical properties from flexibility matrix.

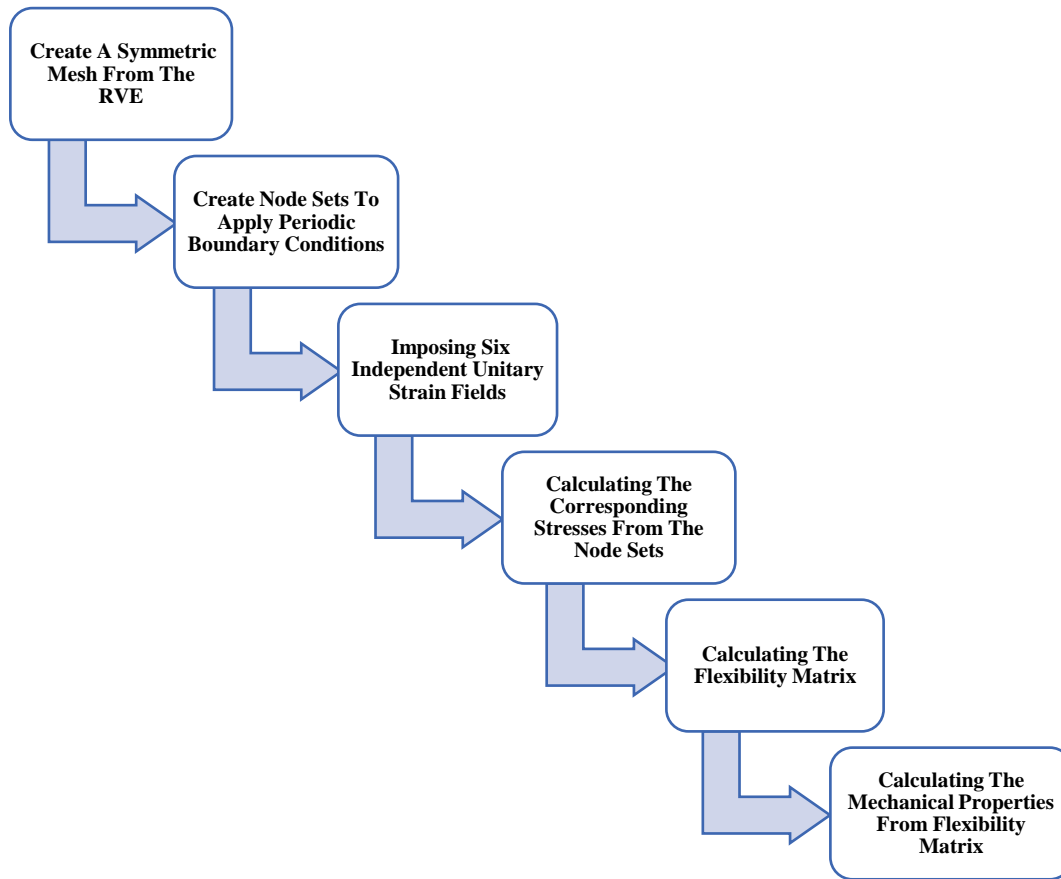


Fig. 9. A summary of the steps required to calculate the spatial properties of porous materials using the method presented in this article

RESULTS

This section presents the results of numerical analyses used to calculate the mechanical properties of porous materials using the method described in the previous section. In addition, to validate the numerical analysis, the results of this article are compared with those presented in reference [56, 57]. Figures 11 to 16 depict, respectively, the change in relative elasticity modulus and relative shear modulus of porous material as a percentage of porosity. According to these graphs, the value of the modulus of elasticity and the relative shear modulus of a porous material decreases nonlinearly as the percentage of porosity increases, with approximately 25% of the modulus of elasticity and shear remaining at a porosity level of 55%. Extrapolating the graph reveals that at approximately 80% porosity, the porous material's modulus of elasticity and shear tend toward zero, indicating that the porous material will lose its mechanical strength. Comparing the results of this study with those presented in reference [56] reveals a good correlation between the values of the modulus of elasticity and the relative shear calculated. This agreement indicates that the modeling and analysis process

used to calculate the mechanical properties of porous materials in this article is accurate. In this context, all calculated mechanical properties have been compared with results of Marco et al. [56] and Zerhouni et al. [57].

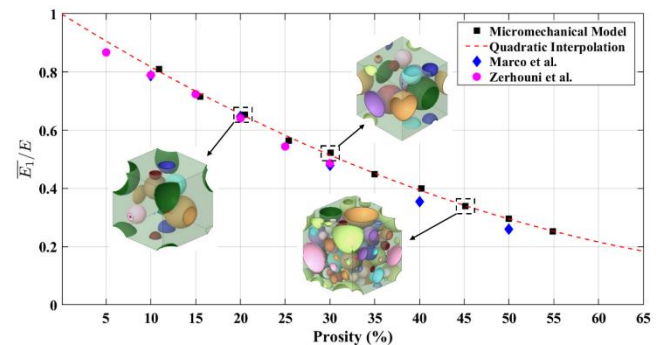


Fig. 10. Relative Longitudinal Young's Modulus (\bar{E}_1/E) for different porosities

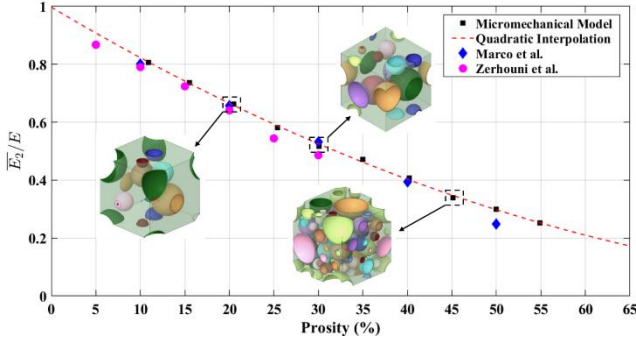


Fig. 11. Relative Transversal Young's Modulus (\bar{E}_2/E) for different porosities

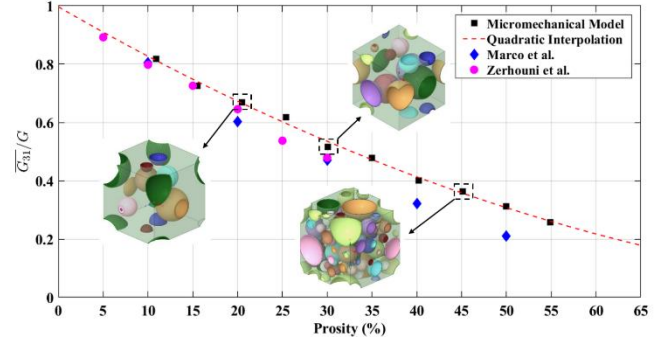


Fig. 15. Relative Out of plane shear modulus (\bar{G}_{31}/G) for different porosities

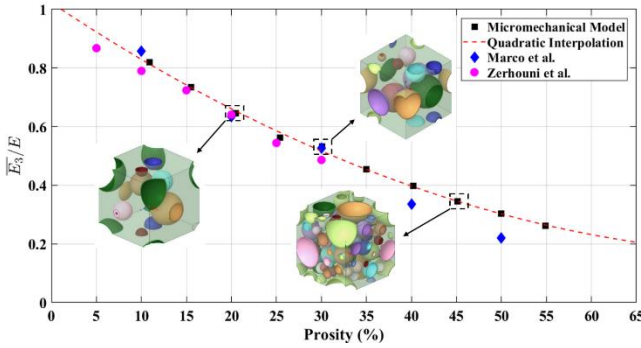


Fig. 12. Relative Transversal Young's Modulus (\bar{E}_3/E) for different porosities

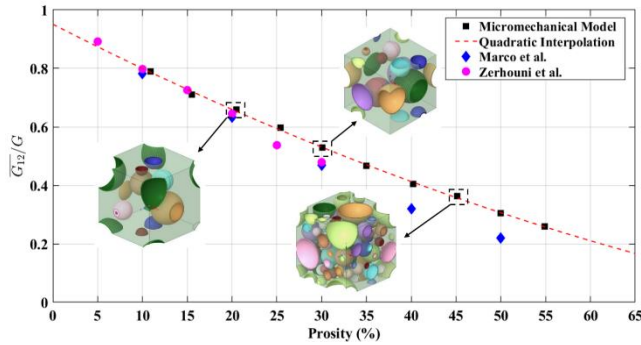


Fig. 13. Relative In-plane shear modulus (\bar{G}_{12}/G) for different porosities

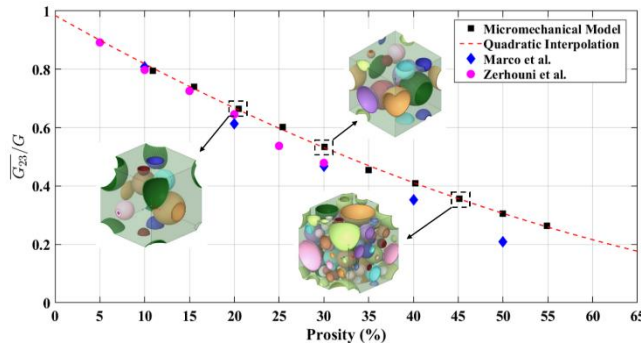


Fig. 14. Relative Out of plane shear modulus (\bar{G}_{23}/G) for different porosities

CONCLUSIONS

Take in to account of several application of porous materials, a precise examination of the mechanical properties of pores seems necessary. In this study, the novel numerical method has been proposed for estimation of mechanical behavior of porous materials as a function of the porosity configuration. In this regard, a MATLAB script was developed for geometrical modeling of porous material in Micro/Meso Scale and each pore's position and radius are chosen randomly within a predetermined tolerance range. The porous never overlap by setting the minimum distance criterion to twice the radius. Also, the user allows adjusting the size of the boundary cube, the sphere's radius, and the total number of spheres. Furthermore, several porous configurations are simulated using finite element method to estimated mechanical properties of porous materials. In addition, periodic boundary conditions have been employed for calculation of stiffness matrix on different RVE and the effects of different parameter like shape, number and size of pores have been investigated on mechanical behavior of porous materials. The results demonstrate that high range of porosity (from 5% to 65%) has been modeled. Also, it can estimate the effective constant of porous materials in 3 directions including of ($E_1, E_2, E_3, G_{12}, G_{13}, G_{23}$).

REFERENCES

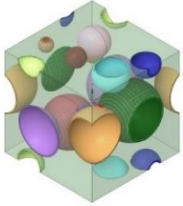
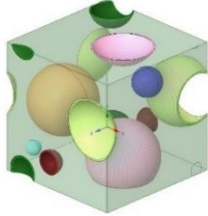
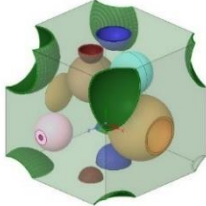
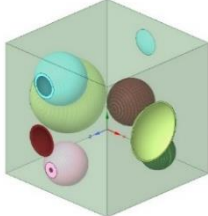
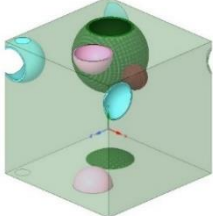
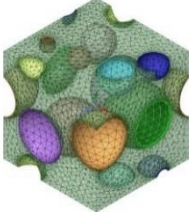
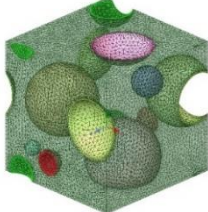
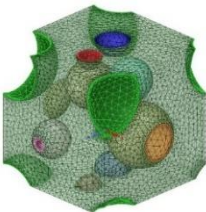
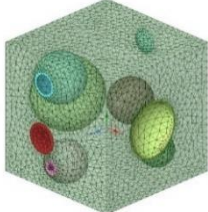
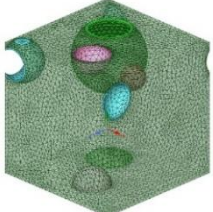
- [1] Linul E, Marsavina L. Assesment of sandwich beams with rigid polyurethane foam core using failure-mode maps. Proc. Romanian Acad. A. 2015 Oct 1;16(4):522-30.
- [2] Sharafi P, Nemati S, Samali B, Mousavi A, Khakpour S, Aliabadizadeh Y. Edgewise and flatwise compressive behaviour of foam-filled sandwich panels with 3-D high density polyethylene skins. Engineering Solid Mechanics. 2018;6(3):285-98.
- [3] Aliha MR, Linul E, Bahmani A, Marsavina L. Experimental and theoretical fracture toughness investigation of PUR foams under mixed mode I+ III loading. Polymer Testing. 2018 May 1;67:75-83.
- [4] Xu Z, Hao H. Electromagnetic interference shielding effectiveness of aluminum foams with different

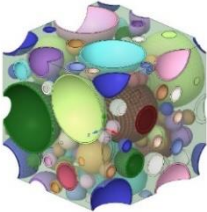
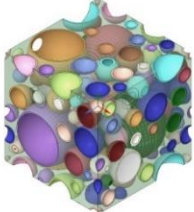

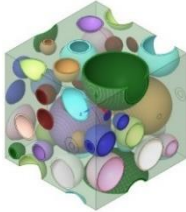
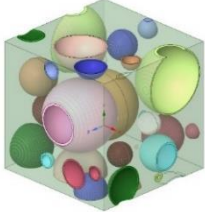
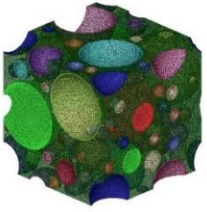
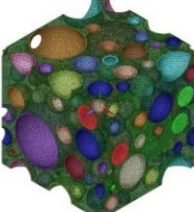


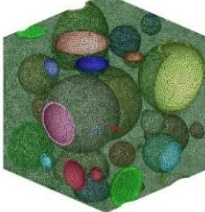
- porosity. *Journal of Alloys and compounds*. 2014 Dec 25;617:207-13.
- [5] Zieliński TG. Numerical investigation of active porous composites with enhanced acoustic absorption. *Journal of Sound and Vibration*. 2011 Oct 24;330(22):5292-308.
- [6] Compston P, Styles M, Kalyanasundaram S. Low energy impact damage modes in aluminum foam and polymer foam sandwich structures. *Journal of Sandwich Structures & Materials*. 2006 Sep;8(5):365-79.
- [7] Kavi H, Toksoy AK, Guden M. Predicting energy absorption in a foam-filled thin-walled aluminum tube based on experimentally determined strengthening coefficient. *Materials & design*. 2006 Jan 1;27(4):263-9.
- [8] Linul E, Vălean C, Linul PA. Compressive behavior of aluminum microfibers reinforced semi-rigid polyurethane foams. *Polymers*. 2018 Nov 23;10(12):1298.
- [9] Sharafi P, Nemati S, Samali B, Bahmani A, Khakpour S, Aliabadizadeh Y. Flexural and shear performance of an innovative foam-filled sandwich panel with 3-D high density polyethylene skins. *Engineering Solid Mechanics*. 2018:113-28.
- [10] Voiconi T, Negru R, Linul E, Marsavina L, Filipescu H. The notch effect on fracture of polyurethane materials. *Frattura ed Integrità Strutturale*. 2014 Sep 8;8(30):101-8.
- [11] Linul E, Serban DA, Marsavina L. Influence of cell topology on mode I fracture toughness of cellular structures. *Physical Mesomechanics*. 2018 Mar;21:178-86.
- [12] Marsavina L, Linul E, Voiconi T, Sadowski T. A comparison between dynamic and static fracture toughness of polyurethane foams. *Polymer Testing*. 2013 Jun 1;32(4):673-80.
- [13] Negru R, Marsavina L, Voiconi T, Linul E, Filipescu H, Belgiu G. Application of TCD for brittle fracture of notched PUR materials. *Theoretical and Applied Fracture Mechanics*. 2015 Dec 1;80:87-95.
- [14] Khansari NM, Fakoor M, Berto F. Probabilistic micromechanical damage model for mixed mode I/II fracture investigation of composite materials. *Theoretical and Applied Fracture Mechanics*. 2019 Feb 1;99:177-93.
- [15] Mehri Khansari NA. Micro-mechanical damage model for obtaining mixed mode I/II fracture criteria in orthotropic materials considering uncertainty approach in University of Tehran. 2019, University of Tehran: Tehran. p. 189.
- [16] Bruggeman VD. Berechnung verschiedener physikalischer Konstanten von heterogenen Substanzen. I. Dielektrizitätskonstanten und Leitfähigkeiten der Mischkörper aus isotropen Substanzen. *Annalen der physik*. 1935;416(7):636-64.
- [17] Boccaccini AR, Fan Z. A new approach for the Young's modulus-porosity correlation of ceramic materials. *Ceramics International*. 1997 Jan 1;23(3):239-45.
- [18] Pal R. Porosity-dependence of effective mechanical properties of pore-solid composite materials. *Journal of Composite Materials*. 2005 Jul;39(13):1147-58.
- [19] Mooney M. The viscosity of a concentrated suspension of spherical particles. *Journal of colloid science*. 1951 Apr 1;6(2):162-70.
- [20] Krieger IM, Dougherty TJ. A mechanism for non-Newtonian flow in suspensions of rigid spheres. *Trans. Soc. Rheol*. 1959 Mar 1;3(1):137-52.
- [21] Walpole LJ. The elastic field of an inclusion in an anisotropic medium. *Proceedings of the Royal Society of London. Series A. Mathematical and Physical Sciences*. 1967 Aug 30;300(1461):270-89.
- [22] Eshelby JD. The determination of the elastic field of an ellipsoidal inclusion, and related problems. *Proceedings of the royal society of London. Series A. Mathematical and physical sciences*. 1957 Aug 20;241(1226):376-96.
- [23] Willis JR. The stress field around an elliptical crack in an anisotropic elastic medium. *International Journal of Engineering Science*. 1968 Jun 1;6(5):253-63.
- [24] Mura T, Lin S. Thin inclusions and cracks in anisotropic media. *Journal of Applied Mechanics*, 1974;41(1):209-14.
- [25] Kassir MK, Sih GC. Three-dimensional stresses around elliptical cracks in transversely isotropic solids. *Engineering fracture mechanics*. 1968 Aug 1;1(2):327-45.
- [26] Ghahremani F. Numerical evaluation of the stresses and strains in ellipsoidal inclusions in an anisotropic elastic material. *Mechanics Research Communications*. 1977 Jan 1;4(2):89-91.
- [27] Irwin GR. Crack-extension force for a part-through crack in a plate. *Journal of Applied Mechanics*, 1962;29(4):651-4.
- [28] Budiansky B, O'connell RJ. Elastic moduli of a cracked solid. *International journal of Solids and structures*. 1976 Jan 1;12(2):81-97.
- [29] Hoening A. Near-tip behavior of a crack in a plane anisotropic elastic body. *Engineering Fracture Mechanics*. 1982 Jan 1;16(3):393-403.
- [30] Hoening A. The behavior of a flat elliptical crack in an anisotropic elastic body. *International Journal of Solids and Structures*. 1978 Jan 1;14(11):925-34.
- [31] Mori T, Tanaka K. Average stress in matrix and average elastic energy of materials with misfitting inclusions. *Acta metallurgica*. 1973 May 1;21(5):571-4.
- [32] Hashin Z. The differential scheme and its application to cracked materials. *Journal of the Mechanics and Physics of Solids*. 1988 Jan 1;36(6):719-34.
- [33] Huang JH, Liu HK. On a flat ellipsoidal inclusion or crack in three-dimensional anisotropic media. *International journal of engineering science*. 1998 Jan 1;36(2):143-55.
- [34] Christensen RM, Lo K. Solutions for effective shear properties in three phase sphere and cylinder models.

- Journal of the Mechanics and Physics of Solids. 1979 Aug 1;27(4):315-30.
- [35]Feng XQ, Yu SW. Estimate of effective elastic moduli with microcrack interaction effects. Theoretical and applied fracture mechanics. 2000 Nov 1;34(3):225-33.
- [36]Bristow JR. Microcracks, and the static and dynamic elastic constants of annealed and heavily cold-worked metals. British Journal of Applied Physics. 1960 Feb 1;11(2):81.
- [37]Mehri Khansari N, Aliha MR. Mixed-modes (I/III) fracture of aluminum foam based on micromechanics of damage. International Journal of Damage Mechanics. 2023 Apr;32(4):519-48.
- [38]Ataei-Aazam M, Safarabadi M, Beygzade M, Khansari NM. Numerical & experimental assessment of mixed-modes (I/II) fracture of PMMA/hydroxyapatite nanocomposite. Theoretical and Applied Fracture Mechanics. 2023 Feb 1;123:103737.
- [39]Ganjiani M, Safarabadi M, Mehri-Khansari N, Oruji H. Effects of delamination in drilling glass/polyester composite. Frontiers of Structural and Civil Engineering. 2021 Apr;15(2):552-67.
- [40]Fakoore M, Sabour M, Khansari N. A new approach for investigation of damage zone properties in orthotropic materials. Engineering Solid Mechanics. 2014;2(4):283-92.
- [41]Budiansky B, O'connell RJ. Elastic moduli of a cracked solid. International journal of Solids and structures. 1976 Jan 1;12(2):81-97.
- [42]Hashin Z. The differential scheme and its application to cracked materials. Journal of the Mechanics and Physics of Solids. 1988 Jan 1;36(6):719-34.
- [43]Huang Y, Hu KX, Wei X, Chandra A. A generalized self-consistent mechanics method for composite materials with multiphase inclusions. Journal of the Mechanics and Physics of Solids. 1994 Mar 1;42(3):491-504.
- [44]Sumarac D, Krajcinovic D. A self-consistent model for microcrack-weakened solids. Mechanics of Materials. 1987 Mar 1;6(1):39-52.
- [45]Feng XQ, Yu SW. Estimate of effective elastic moduli with microcrack interaction effects. Theoretical and applied fracture mechanics. 2000 Nov 1;34(3):225-33.
- [46]Fakoore M, Khansari NM. Mixed mode I/II fracture criterion for orthotropic materials based on damage zone properties. Engineering Fracture Mechanics. 2016 Mar 1;153:407-20.
- [47]Mehri Khansari N, Aliha MR. Mixed-modes (I/III) fracture of aluminum foam based on micromechanics of damage. International Journal of Damage Mechanics. 2023 Apr;32(4):519-48.
- [48]Unger JF, Eckardt S. Multiscale modeling of concrete: from mesoscale to macroscale. Archives of computational Methods in Engineering. 2011 Sep;18:341-93.
- [49]Fishman GS, Moore LR. A statistical evaluation of multiplicative congruential random number generators with modulus 231—1. Journal of the American Statistical Association. 1982 Mar 1;77(377):129-36.
- [50]Unger JF, Eckardt S. Multiscale modeling of concrete: from mesoscale to macroscale. Archives of computational Methods in Engineering. 2011 Sep;18:341-93.
- [51]Salman BF, Al-Rumaithi A, Al-Sherrawi MH. Properties of reactive powder concrete with different types of cement. IJCIET. 2018 Oct;9(10):1313-21.
- [52]Shehata F, ElMahallawy N, Arab M, Agwa M. Equal channel angular pressing of Al-SiC composites fabricated by stir casting. Open Journal of Metal. 2013 Jul 16;3(02):26.
- [53]Peng C, Tran P, Nguyen-Xuan H, Ferreira AJ. Mechanical performance and fatigue life prediction of lattice structures: Parametric computational approach. Composite Structures. 2020 Mar 1;235:111821.
- [54]Reisinger AG, Pahr DH, Zysset PK. Elastic anisotropy of bone lamellae as a function of fibril orientation pattern. Biomechanics and Modeling in Mechanobiology. 2011 Feb;10:67-77.
- [55]Marco M, Belda R, Miguélez MH, Giner E. Numerical analysis of mechanical behaviour of lattice and porous structures. Composite Structures. 2021 Apr 1;261:113292.
- [56]Zerhouni O, Tarantino MG, Danas K. Numerically-aided 3D printed random isotropic porous materials approaching the Hashin-Shtrikman bounds. Composites Part B: Engineering. 2019 Jan 1;156:344-54.

APPENDIX

Table 2. Summary of the different modes investigated to calculate the mechanical properties of porous materials

| Case 5 | Case 4 | Case 3 | Case 2 | Case 1 | Properties |
|---|---|---|---|---|-----------------------|
| 30.1% | 25.4% | 20.5% | 15.5% | 10.9% | Porosity |
| Aluminum | Aluminum | Aluminum | Aluminum | Aluminum | Base Metal |
| Sphere | Sphere | Sphere | Sphere | Sphere | Type of pores |
| 0.5 to 3 μm | 0.5 to 3 μm | 0.5 to 3 μm | 0.5 to 3 μm | 0.5 to 3 μm | Diameter of sphere |
| Random | Random | Random | Random | Random | Distribution of pores |
|  |  |  |  |  | Geometry |
|  |  |  |  |  | Mesh |
| $E_1 = 37.079 \text{ GPa}$ $E_2 = 36.713 \text{ GPa}$ $E_3 = 37.745 \text{ GPa}$ $G_{12} = 14.101 \text{ GPa}$ $G_{23} = 14.278 \text{ GPa}$ $G_{31} = 13.754 \text{ GPa}$ | $E_1 = 40.095 \text{ GPa}$ $E_2 = 41.253 \text{ GPa}$ $E_3 = 39.989 \text{ GPa}$ $G_{12} = 15.937 \text{ GPa}$ $G_{23} = 16.061 \text{ GPa}$ $G_{31} = 16.490 \text{ GPa}$ | $E_1 = 46.349 \text{ GPa}$ $E_2 = 46.977 \text{ GPa}$ $E_3 = 45.843 \text{ GPa}$ $G_{12} = 17.597 \text{ GPa}$ $G_{23} = 17.714 \text{ GPa}$ $G_{31} = 17.862 \text{ GPa}$ | $E_1 = 50.824 \text{ GPa}$ $E_2 = 52.309 \text{ GPa}$ $E_3 = 52.157 \text{ GPa}$ $G_{12} = 18.981 \text{ GPa}$ $G_{23} = 19.758 \text{ GPa}$ $G_{31} = 19.355 \text{ GPa}$ | $E_1 = 57.517 \text{ GPa}$ $E_2 = 57.249 \text{ GPa}$ $E_3 = 58.120 \text{ GPa}$ $G_{12} = 21.060 \text{ GPa}$ $G_{23} = 21.225 \text{ GPa}$ $G_{31} = 21.845 \text{ GPa}$ | Mechanical Properties |

| Case 10 | Case 9 | Case 8 | Case 7 | Case 6 | Properties |
|--|--|--|---|---|-----------------------|
| 54.9% | 50.0% | 45.1% | 40.2% | 35.0% | Porosity |
| Aluminum | Aluminum | Aluminum | Aluminum | Aluminum | Base Metal |
| Sphere | Sphere | Sphere | Sphere | Sphere | Type of pores |
| 0.5 to 3 μm | 0.5 to 3 μm | 0.5 to 3 μm | 0.5 to 3 μm | 0.5 to 3 μm | Diameter of sphere |
| Random | Random | Random | Random | Random | Distribution of pores |
|  |  |  |  |  | Geometry |
|  |  |  |  |  | Mesh |
| $E_1 = 17.861 \text{ GPa}$ $E_2 = 17.970 \text{ GPa}$ $E_3 = 18.537 \text{ GPa}$ $G_{12} = 6.928 \text{ GPa}$ $G_{23} = 7.045 \text{ GPa}$ $G_{31} = 6.895 \text{ GPa}$ | $E_1 = 20.947 \text{ GPa}$ $E_2 = 21.246 \text{ GPa}$ $E_3 = 21.584 \text{ GPa}$ $G_{12} = 8.112 \text{ GPa}$ $G_{23} = 8.147 \text{ GPa}$ $G_{31} = 8.327 \text{ GPa}$ | $E_1 = 24.087 \text{ GPa}$ $E_2 = 24.096 \text{ GPa}$ $E_3 = 24.524 \text{ GPa}$ $G_{12} = 9.674 \text{ GPa}$ $G_{23} = 9.499 \text{ GPa}$ $G_{31} = 9.697 \text{ GPa}$ | $E_1 = 28.452 \text{ GPa}$ $E_2 = 28.866 \text{ GPa}$ $E_3 = 28.300 \text{ GPa}$ $G_{12} = 10.803 \text{ GPa}$ $G_{23} = 10.917 \text{ GPa}$ $G_{31} = 10.714 \text{ GPa}$ | $E_1 = 31.871 \text{ GPa}$ $E_2 = 33.481 \text{ GPa}$ $E_3 = 32.225 \text{ GPa}$ $G_{12} = 12.447 \text{ GPa}$ $G_{23} = 12.115 \text{ GPa}$ $G_{31} = 12.777 \text{ GPa}$ | Mechanical Properties |